IMPACT OF PARTONIC AND HADRONIC TRANSPORT PROCESSES ON ELLIPTIC FLOW IN THE AMPT MODEL

Yao Zhang

School of Energy and Mechanical Engineering
Jiangxi University of Science and Technology
Nanchang 330013, China

Received 8 June 2025, accepted 17 November 2025, published online 27 November 2025

The AMPT model is used to study elliptic flow v_2 in Au+Au collisions at $\sqrt{s_{NN}} = 200$ GeV, focusing on partonic and hadronic transport processes. By varying the partonic elastic scattering cross section σ_p and scaling hadronic cross sections σ_H, we find that v_2 is dominated by partonic interactions with larger σ_p accelerating momentum-space anisotropy conversion and suppressing residual spatial anisotropy. Hadronic rescattering minimally impacts v_2, only emerging at reduced σ_p and higher centrality. The results highlight the critical role of partonic transport in collective flow and the limited influence of hadronic dynamics on final observables.

DOI:10.5506/APhysPolB.56.12-A3

1. Introduction

In relativistic heavy-ion collisions, the collective behavior of produced matter provides critical insights into the properties of the deconfined quark–gluon plasma (QGP) and its transition to hadronic matter under extreme conditions [1–7]. Among the key observables, elliptic flow v_2, which quantifies the azimuthal anisotropy of particle emission, serves as a sensitive probe of the early-stage pressure gradients and transport dynamics of the system [8–11]. The magnitude of v_2 reflects the interplay between the initial geometric anisotropy of the collision and the subsequent thermalization and viscous effects during the evolution of the system [12, 13]. Understanding the relative contributions of partonic and hadronic transport processes to v_2 is therefore essential for disentangling the roles of QGP formation and hadronic rescattering in shaping final-state observables.

The AMPT (A Multi-Phase Transport) model highlights the microscopic mechanisms driving momentum-space anisotropy, while hydrodynamic simulations emphasize the near-perfect fluidity of the QGP [8, 11, 14–16]. Previous studies have established that partonic scattering plays a dominant role in

generating v_2 [17–21]. However, the extent to which hadronic rescattering modifies residual anisotropy or redistributes momentum remains debated. Existing works often focus on either partonic or hadronic dynamics, leaving their combined effects underexplored. For instance, while a larger partonic elastic scattering cross section is known to enhance v_2 by accelerating the conversion of spatial anisotropy into momentum anisotropy, the influence of hadronic scattering cross section on final-state observables remains ambiguous due to the complexity of cross sections across numerous hadronic channels. Addressing these gaps is critical for refining interpretations of experimental data and constraining transport coefficients such as shear viscosity. In this work, we investigate the differential impacts of partonic and hadronic transport processes on v_2 in Au+Au collisions at $\sqrt{s_{NN}} = 200$ GeV using the AMPT model. Section 2 outlines the transport processes and parameter configurations of partons and hadrons in the AMPT model. Section 3 presents the results on v_2 compared to experimental data. Conclusions are summarized in Section 4.

2. Transport processes of partons and hadrons in AMPT

The AMPT model is a hybrid model for generating heavy-ion collision events, which includes the initial conditions, partonic interactions, hadronization, and hadronic interactions [8]. The transport processes of partons and hadrons based on non-equilibrium dynamics are described by the ZPC and ART cascade models, respectively. The partonic cascade includes only two-body scatterings and treats partonic interactions at a distance $\sqrt{\sigma_p/\pi}$ used for solving the Boltzmann equations. The partonic elastic scattering cross section is $\sigma_p \approx \frac{9\pi\alpha_s^2}{2\mu^2}$ which can be adjusted by changing the strong coupling constant α_s and the screening mass μ, and can be used in studying the influence of partonic transport processes in the model.

The hadronic cascade includes hadron elastic and inelastic scatterings which exhibit varying hadronic scattering cross sections σ_H across different hadronic scattering channels. Many of the hadronic cross sections used in the model have not been thoroughly studied theoretically and have not been adequately constrained by experimental data. Similar to partonic scattering, the occurrence of hadronic scattering collisions is conditioned by their separation distance being smaller than the maximum collision distance, which scales with the square root of σ_H. However, unlike σ_p that can be directly adjusted within the model, the hadronic cascade contains numerous scattering channels with distinct cross sections, making it impossible to globally regulate σ_H by modifying individual channel cross sections. To study the influence of hadronic transport processes, a proportional adjustment of all hadronic cross sections can be equivalently realized by uniformly increasing

the maximum collision distance across all scattering channels [22]. Notably, scaling factors of 2 times in the maximum collision distance equate to 4 times amplification in σ_H.

The tuning of partonic and hadronic cross sections enables the investigation of transport dynamics within the model. Both σ_p and σ_H are the most critical parameters in transport processes, not only determining the shear viscosity properties of partonic and hadronic matter, respectively, but also directly affecting the results of final-state observables [19–21, 23–25]. For a fixed scattering cross section, the specific shear viscosity exhibits a rapid increase with decreasing temperature [23]. The transport process overestimates the shear viscosity of partonic and hadronic matter, especially near the phase transition temperature. The shear viscosity significantly exceeds the value estimated by viscous relativistic hydrodynamic simulations close to the KSS bound in relativistic heavy-ion collisions [26–28]. Considering the inverse relationship between scattering cross section and shear viscosity, using transport simulations with larger σ_p and σ_H can reflect the impact of smaller shear viscosity on final observables. To see the effect of partonic and hadronic interactions, heavy-ion collision events in the AMPT model are generated with $\sigma_p = 3$, 6, 9 mb and the hadronic cross sections that are 4 times the default σ_H of all hadrons for comparison. The parameters of the Lund string fragmentation $a_{\mathrm{L}} = 0.55$ and $b_{\mathrm{L}} = 0.2$ GeV^{-2}, $\alpha_{\mathrm{s}} = 0.33$ are chosen for Au+Au collisions at $\sqrt{s_{NN}} = 200$ GeV in the model, which correspond to the default settings in the string melting version (v2.26t5) of the AMPT model. A smaller b_{L} enhances the effective string tension, leading to a larger mean transverse momentum for the initial quarks after string melting and, consequently, better agreement with experimental findings.

Figures 1 and 2 show the charged hadron pseudorapidity spectra and transverse momentum spectra, respectively, with various σ_p and σ_H for Au+Au collisions at $\sqrt{s_{NN}} = 200$ GeV compared to the BRAHMS and STAR data at various centralities. Both, $\mathrm{d}N/\mathrm{d}\eta$ pseudorapidity distribution and p_{T} spectra of charged hadron are well reproduced at all centralities in the model. It can be seen that increasing σ_p significantly reduces the particle yield at mid-pseudorapidity, while σ_H exhibits a weaker influence on the pseudorapidity spectrum compared to σ_p, with its significance becoming pronounced only when σ_p is small. The effect of varying scattering cross sections on $\mathrm{d}N/\mathrm{d}\eta$ pseudorapidity distribution is linked to the viscous properties of the system. Reduced cross sections increase shear viscosity, which suppresses longitudinal expansion and elevates mid-pseudorapidity particle yields. The weaker impact of σ_H compared to σ_p arises because the early rapid expansion of the system relies on partonic scattering, while hadronic rescattering provides weaker driving force for further expansion of a hadronized and rapidly expanding system. It should be noted that in the

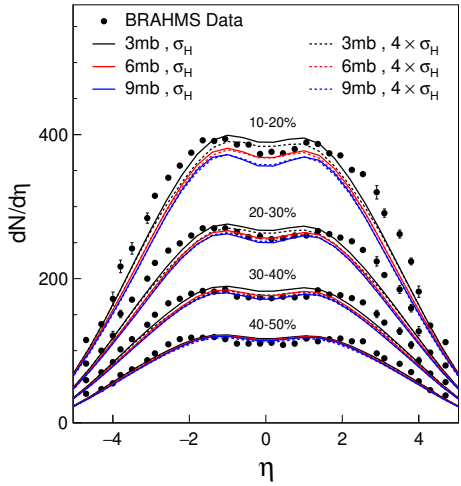

Fig. 1. The charged hadron pseudorapidity spectra for Au+Au collisions at $\sqrt{s_{NN}} = 200$ GeV with various σ_p and σ_H in different centrality classes compared to experimental data from the BRAHMS Collaboration [29].

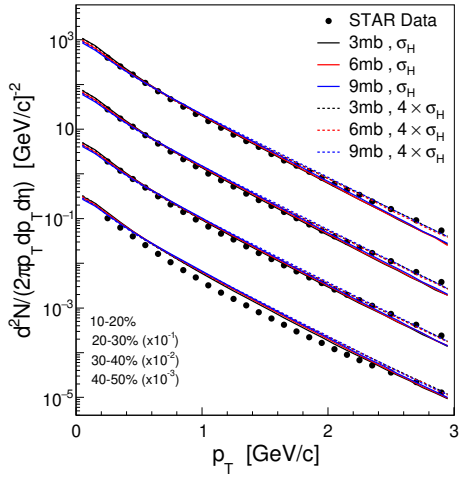

Fig. 2. The transverse momentum spectra of mid-pseudorapidity charged hadrons with various σ_p and σ_H in different centrality classes compared to experimental data from the STAR Collaboration [30]. Curves from top to bottom correspond to 10–20%, 20–30%, 30–40%, and 40–50% centralities, respectively.

model, parton scattering includes only two-body elastic scattering, whereas hadron scattering encompasses both elastic and inelastic processes. An enlarged elastic scattering cross section promotes longitudinal expansion of the system, which suppresses the particle yield at mid-pseudorapidity, while the accompanying inelastic scattering channels generate additional hadrons.

A small σ_p leads to a shorter evolution duration for the partonic phase, thereby amplifying the role of hadronic scattering in driving system expansion. This results in a reduction of the mid-pseudorapidity particle yield, chiefly caused by the strengthened longitudinal expansion. With increasing σ_p, the prolonged evolution time of the partonic system reduces the influence of hadronic scattering on expansion, causing the increased hadron production from hadronic inelastic scattering to gradually dominate. As reflected in Fig. 1, a noticeable suppression of the mid-pseudorapidity particle yield by an increased σ_H occurs only for small σ_p. For larger σ_p, the mid-pseudorapidity does not decrease significantly and instead exhibits a slight rising tendency.

The transverse spectra are minimally affected by partonic and hadronic scattering, where partonic scattering exerts a slight influence on low p_{T} while hadronic scattering shows a comparably limited effect on high p_{T}. The average transverse momentum of both partons after string melting and the final hadrons are mainly influenced by the Lund string fragmentation parameters in the model, whereas the slope of transverse momentum spectra arises from both radial flow and thermalized temperature, exhibiting limited sensitivity to partonic and hadronic scattering interactions. σ_p negligibly affects p_{T} spectra, because the small current quark masses in the model weaken parton coupling to radial flow effects. Nevertheless, at low transverse momentum ($p_{\mathrm{T}} < 0.4$ GeV/c), the abundance of low-p_{T} hadrons is found to decrease with rising σ_p, aligning with the trend observed for mid-pseudorapidity particle production in Fig. 1. Diminished viscosity drives particles to predominantly undergo longitudinal expansion, depleting particle populations at mid-pseudorapidity, particularly those with low p_{T}. While this effect appears subdued in logarithmic scaling, it manifests as a significant modification to the overall particle production yield. By prolonging hadronic evolution and reducing freeze-out temperature, hadronic rescattering enhances hadron yields at high p_{T}, while suppressing production at low p_{T}, and elevated σ_H induces a marginal reduction in the inverse slope of the spectra.

3. Elliptic flow under different scattering cross sections

Anisotropic flow, which can be characterized by flow harmonics of the particle azimuthal angle distribution, originates from pressure gradients induced by the initial geometry of the collision. It is sensitive to the transport properties and processes of the system, where the second harmonic coefficient, elliptic flow v_2, represents a key measurable quantity. The time evolutions of partonic system elliptic flow $v_2 = \langle \frac{p_x^2 - p_y^2}{p_x^2 + p_y^2} \rangle$ and eccentricity

$\varepsilon_2 = \langle \frac{y^2-x^2}{y^2+x^2} \rangle$ in the model are shown in Fig. 3. As the system evolves temporally, the diminishing ε_2 and rising v_2 signify the transfer of anisotropy from the coordinate space to momentum space through partonic transport dynamics. Partonic scattering strongly drives and significantly enhances this conversion, with a larger σ_p leading to faster reductions in ε_2 and more rapid rises in v_2. The elliptic flow in the partonic system, influenced by σ_p, is manifested not only during the evolution of hadronic system but also exerts a direct impact on the final-state v_2.

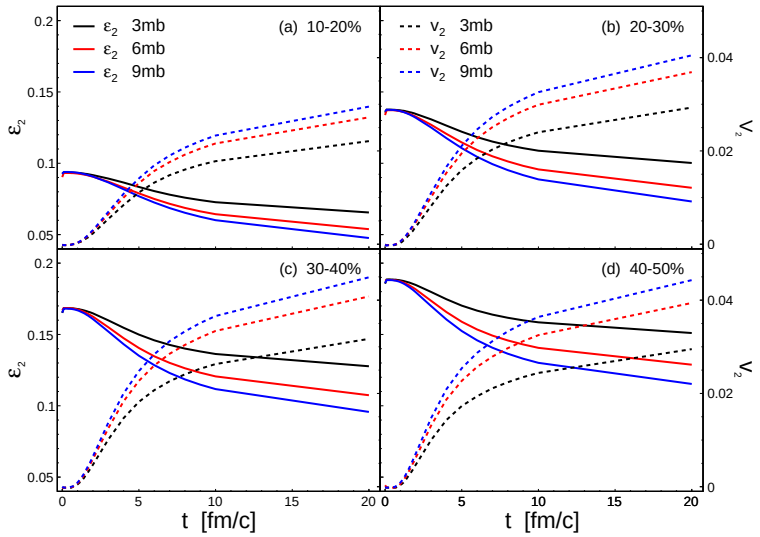

Fig. 3. The time evolutions of partonic system elliptic flow v_2 and eccentricity ε_2 with various σ_p in different centrality classes.

Figure 4 shows the time evolution of hadronic system v_2 with various σ_p and σ_H in different centrality classes. The elliptic flow of the hadronic system progressively approaches saturation with temporal evolution. Increased σ_p not only delays the saturation but also amplifies the saturated v_2, with the variation of saturated flow value exhibiting consistency in trend with the dynamical evolution of the partonic system. Notably, during the initial system prior to flow saturation, a reduced σ_p accelerates the temporal evolution of v_2 and enhances its magnitude. This occurs because a smaller σ_p shortens the partonic phase evolution, leading to an earlier hadronization time. Consequently, hadrons are produced earlier, causing a rapid increase in the flow value during the early stages of the hadronic system. While σ_p exhibits a dominant effect on the v_2 evolution in the hadronic system, the role of σ_H remains marginal, with observable effects emerging solely when σ_p is reduced and collision centrality is elevated.

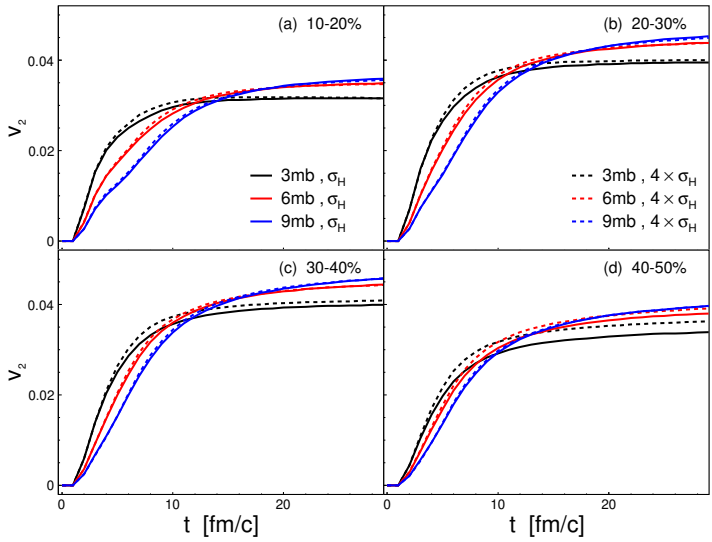

Fig. 4. The time evolution of hadronic system v_2 with various σ_p and σ_H.

Figures 5 and 6 show the charged hadron elliptic flow, which is calculated with the two-particle cumulant method as $v_2 = \sqrt{\langle \cos 2(\phi_1 - \phi_2) \rangle}$, as a function of the transverse momentum and the pseudorapidity, respectively. The final-state hadron v_2 exhibits consistency with the flow value evolution in both partonic and hadronic systems. Compared to the pronounced impact of σ_p on v_2, the influence of σ_H on flow values remains weaker, showing significant effects only when σ_p is small and centrality is high. The observed dependence of σ_H on v_2, linked to σ_p and centrality, arises from the anisotropic evolution of the system in the model. Enhanced σ_p during the rapid expansion of the partonic system amplifies pressure gradient dissipation, thereby reducing coordinate-space anisotropy retained in the hadronic system after hadronization. This diminished residual anisotropy restricts the capacity of hadronic rescattering to generate momentum-space anisotropy. Elevated collision centrality enhances both the initial spatial anisotropy and the rapidity of partonic system evolution, resulting in amplified residual spatial anisotropy within the hadronic system that is accessible for conversion via hadronic rescattering. It should be noted that in Fig. 5, except for cases with small σ_p and high eccentricity where an increase in σ_H enhances v_2, varying σ_H in other results not only shows no significant effect on flow values but also leads to unstable and inconsistent magnitude relationships of v_2 across different transverse momentum ranges. This occurs because a larger σ_p during partonic system evolution converts most of the initially small spatial anisotropy in low eccentricity collisions into momentum-space anisotropy. Although hadronic rescattering can continue to drive system

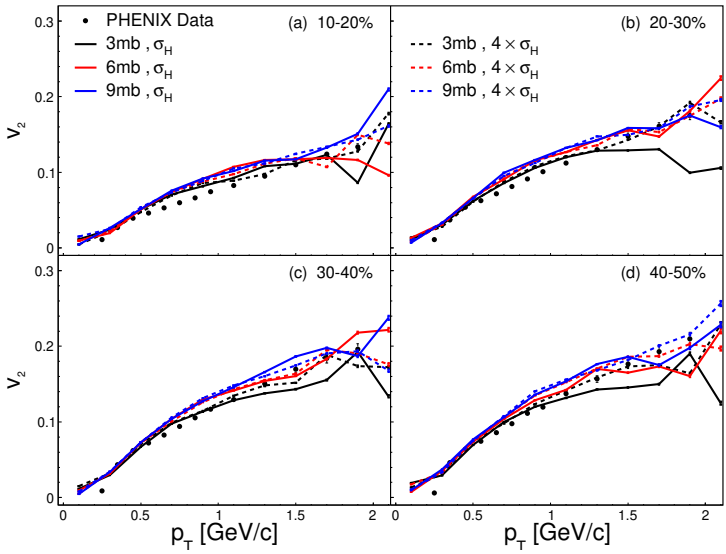

Fig. 5. v_2 of mid-pseudorapidity charged hadrons varies with the transverse momentum with various σ_p and σ_H in different centrality classes compared to experimental data from the PHENIX Collaboration [31].

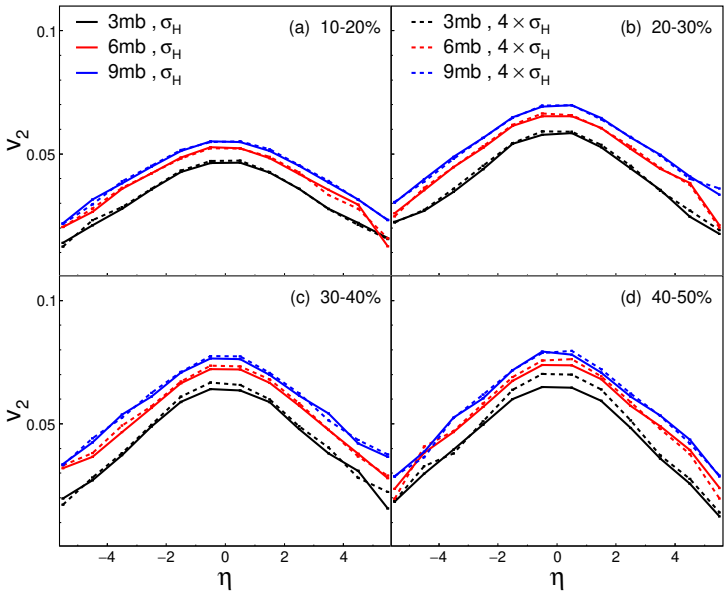

Fig. 6. v_2 of charged hadrons varies with pseudorapidity with various σ_p and σ_H in different centrality classes.

expansion, it does not significantly affect momentum space. Moreover, an increased σ_H enhances inelastic hadronic scattering, the influence of which on momentum space may be the primary cause of flow instabilities. The elliptic flow *versus* transverse momentum is plotted over a relatively wide mid-pseudorapidity interval ($-1 < \eta < 1$) in Fig. 5, whose extensive vertical scale obscures the systematic influence of hadronic rescattering on flow amplitudes. To facilitate clearer observation, Fig. 6 displays the pseudorapidity dependence of v_2 with a constrained vertical range. This magnified scale confirms that enhanced σ_H indeed amplifies v_2 at mid-pseudorapidity specifically in collisions characterized by small σ_p and large centrality.

While hadronic rescattering predominantly modifies momentum-space anisotropy in highly eccentric collisions compared to partonic interactions, it systematically regulates the expansion dynamics and spatial dimensions of the hadronic system over the full centrality spectrum. HBT interferometry presents a viable technique for quantitatively distinguishing the evolutionary imprints of partonic *versus* hadronic scattering processes. The size parameters R_o, R_s, and R_l called HBT radii can be obtained by fitting the HBT correlation function, which is calculated by the Correlation After Burner program without the final-state interactions, with the Bertsch–Pratt parametrization in the 'out–side–long' coordinate system [33, 34]. Figure 7 shows the charged pion HBT radii R_o, R_s, R_l, and the ratio $R_\mathrm{o}/R_\mathrm{s}$ as a function of average transverse momentum in 0–10% centrality with different σ_p and σ_H compared to the PHENIX data. The HBT radii are affected by

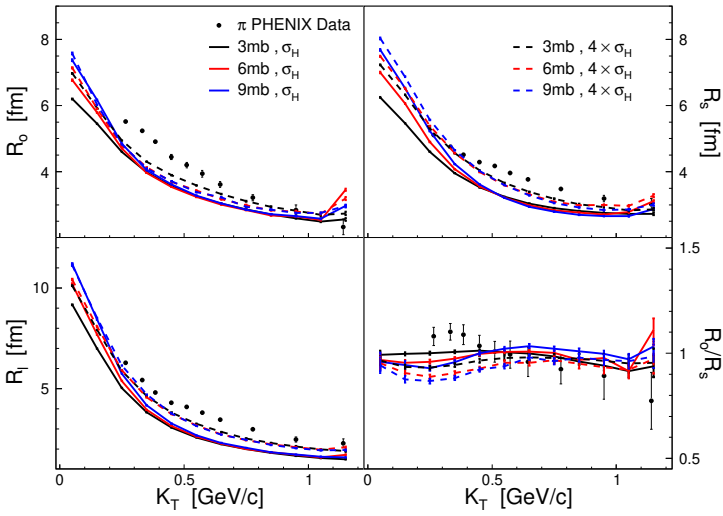

Fig. 7. HBT radii R_o, R_s, R_l, and the ratio $R_\mathrm{o}/R_\mathrm{s}$ of charged pions vary with average transverse momentum with various σ_p and σ_H in 0–10% centrality compared to experimental data from the PHENIX Collaboration [32].

both σ_p and σ_H, notably impacting $R_{\rm s}$ and $R_{\rm l}$. Enhanced cross sections result in radial expansion, with partonic scatterings primarily altering radii at low $p_{\rm T}$, while hadronic scatterings amplify radii across the transverse momentum range. The efficacy of hadronic rescattering is constrained both in transforming residual anisotropy inherited from the partonic system and in reaccelerating the expansion velocity after the initial rapid expansion of the partonic system, thereby making it difficult to exert significant influence on v_2 and $R_{\rm o}$. The marked enhancement of $R_{\rm s}$ and $R_{\rm l}$ is attributable to the extended temporal evolution of the hadronic system, driven by an increase in σ_H.

4. Summary

This study investigates the impact of partonic and hadronic transport processes on elliptic flow within the AMPT model for Au+Au collisions at $\sqrt{s_{NN}} = 200$ GeV. By adjusting the partonic elastic scattering cross section σ_p and scaling the hadronic cross sections σ_H, the interplay between transport dynamics, shear viscosity, and anisotropic flow evolution is systematically analyzed. Enhancing the cross sections of either partons or hadrons produces a unified trend of effects on the final-state particle spectra, elliptic flow, and HBT radii, a phenomenon attributed to the decrease in shear viscosity driven by cross section amplification. The partonic phase, governed by the ZPC cascade, demonstrates a dominant role in driving v_2 through rapid momentum-space anisotropy conversion, with larger σ_p accelerating the growth of v_2 and suppressing residual spatial anisotropy. In contrast, hadronic rescattering, modeled via the ART cascade, exhibits limited influence on v_2, only becoming noticeable at reduced σ_p and higher centrality due to diminished residual anisotropy inherited from the partonic system. Comparisons with experimental data reveal that the pseudorapidity and transverse momentum spectra are primarily shaped by initial conditions and fragmentation parameters, while v_2 shows strong sensitivity to σ_p. The HBT radii further highlight the differential effects: partonic interactions modify radii at low $p_{\rm T}$, whereas hadronic rescattering extends their evolution across $p_{\rm T}$, albeit with minimal impact on v_2. These results underscore the critical role of early partonic transport in governing collective flow, while emphasizing the constrained efficacy of hadronic interactions in altering final-state observables.

This work was supported by the Jiangxi Provincial Key Laboratory of Particle Technology (No. 20242BCC32119) and by the Supercomputing Platform at Jiangxi University of Science and Technology.

REFERENCES

[1] BRAHMS Collaboration (I. Arsene *et al.*), «Quark–gluon plasma and color glass condensate at RHIC? The perspective from the BRAHMS experiment», *Nucl. Phys. A* **757**, 1 (2005).

[2] PHOBOS Collaboration (B.B. Back *et al.*), «The PHOBOS perspective on discoveries at RHIC», *Nucl. Phys. A* **757**, 28 (2005).

[3] PHENIX Collaboration (K. Adcox *et al.*), «Formation of dense partonic matter in relativistic nucleus–nucleus collisions at RHIC: Experimental evaluation by the PHENIX Collaboration», *Nucl. Phys. A* **757**, 184 (2005).

[4] STAR Collaboration (J. Adams *et al.*), «Experimental and theoretical challenges in the search for the quark–gluon plasma: The STAR Collaboration's critical assessment of the evidence from RHIC collisions», *Nucl. Phys. A* **757**, 102 (2005).

[5] P.K. Kovtun, D.T. Son, A.O. Starinets, «Viscosity in Strongly Interacting Quantum Field Theories from Black Hole Physics», *Phys. Rev. Lett.* **94**, 111601 (2005).

[6] U. Heinz, R. Snellings, «Collective Flow and Viscosity in Relativistic Heavy-Ion Collisions», *Annu. Rev. Nucl. Part. Sci.* **63**, 123 (2013).

[7] E. Shuryak, «Strongly coupled quark–gluon plasma in heavy ion collisions», *Rev. Mod. Phys.* **89**, 035001 (2017).

[8] Z.W. Lin *et al.*, «Multiphase transport model for relativistic heavy ion collisions», *Phys. Rev. C* **72**, 064901 (2005).

[9] H. Petersen, «Anisotropic flow in transport + hydrodynamics hybrid approaches», *J. Phys. G: Nucl. Part. Phys.* **41**, 124005 (2014).

[10] S. Ryu *et al.*, «Effects of bulk viscosity and hadronic rescattering in heavy ion collisions at energies available at the BNL Relativistic Heavy Ion Collider and at the CERN Large Hadron Collider», *Phys. Rev. C* **97**, 034910 (2018).

[11] Z.W. Lin, L. Zheng, «Further developments of a multi-phase transport model for relativistic nuclear collisions», *Nucl. Sci. Tech.* **32**, 113 (2021).

[12] N. Borghini, P.M. Dinh, J.Y. Ollitrault, «Flow analysis from multiparticle azimuthal correlations», *Phys. Rev. C* **64**, 054901 (2001).

[13] A. Bilandzic, R. Snellings, S. Voloshin, «Flow analysis with cumulants: Direct calculations», *Phys. Rev. C* **83**, 044913 (2011).

[14] C. Shen, U. Heinz, P. Huovinen, H. Song, «Systematic parameter study of hadron spectra and elliptic flow from viscous hydrodynamic simulations of Au Au collisions at GeV», *Phys. Rev. C* **82**, 054904 (2010).

[15] H. Song *et al.*, «200 *A*GeV Au+Au Collisions Serve a Nearly Perfect Quark–Gluon Liquid», *Phys. Rev. Lett.* **106**, 192301 (2011).

[16] E. Molnar *et al.*, «Influence of temperature-dependent shear viscosity on elliptic flow at backward and forward rapidities in ultrarelativistic heavy-ion collisions», *Phys. Rev. C* **90**, 044904 (2014).

[17] J. Xu, C.M. Ko, «Pb–Pb collisions at $\sqrt{s_{NN}} = 2.76$ TeV in a multiphase transport model», *Phys. Rev. C* **83**, 034904 (2011).

[18] Y. Zhou *et al.*, «Anisotropic distributions in a multiphase transport model», *Phys. Rev. C* **93**, 034909 (2016).

[19] Y. Zhang, J. Zhang *et al.*, «Temperature-independent shear viscosity in a multiphase transport model for relativistic heavy ion collisions», *Phys. Rev. C* **96**, 044914 (2017).

[20] Y. Zhang, Q. Liu, «Shear viscous transport dynamics simulations of parton matter in AMPT model», *Eur. Phys. J. A* **59**, 296 (2023).

[21] Y. Zhang, «Charged hadron spectra and anisotropic flow from the AMPT model with shear viscous transport dynamics simulations at RHIC», *Eur. Phys. J. A* **61**, 15 (2025).

[22] Y. Zhang, «Effect of hadronic transport processes on HBT radii in the AMPT model», *J. Phys. G: Nucl. Part. Phys.* **52**, 055104 (2025).

[23] J. Xu, C.M. Ko, «Triangular flow in heavy ion collisions in a multiphase transport model», *Phys. Rev. C* **84**, 014903 (2011).

[24] A. Wiranata, M. Prakash, «Shear viscosities from the Chapman–Enskog and the relaxation time approaches», *Phys. Rev. C* **85**, 054908 (2012).

[25] N.M. MacKay, Z.W. Lin, «The shear viscosity of parton matter under anisotropic scatterings», *Eur. Phys. J. C* **82**, 918 (2022).

[26] J.E. Bernhard, J.S. Moreland, S.A. Bass, «Bayesian estimation of the specific shear and bulk viscosity of quark–gluon plasma», *Nat. Phys.* **15**, 1113 (2019).

[27] JETSCAPE Collaboration (D. Everett *et al.*), «Phenomenological Constraints on the Transport Properties of QCD Matter with Data-Driven Model Averaging», *Phys. Rev. Lett.* **126**, 242301 (2021).

[28] J.E. Parkkila, A. Onnerstad, D.J. Kim, «Bayesian estimation of the specific shear and bulk viscosity of the quark–gluon plasma with additional flow harmonic observables», *Phys. Rev. C* **104**, 054904 (2021).

[29] BRAHMS Collaboration (I.G. Bearden *et al.*), «Pseudorapidity Distributions of Charged Particles from Au+Au Collisions at the Maximum RHIC Energy, $\sqrt{s_{NN}} = 200$ GeV», *Phys. Rev. Lett.* **88**, 202301 (2002).

[30] STAR Collaboration (J. Adams *et al.*), «Transverse-Momentum and Collision-Energy Dependence of High-p_{T} Hadron Suppression in Au+Au Collisions at Ultrarelativistic Energies», *Phys. Rev. Lett.* **91**, 172302 (2003).

[31] PHENIX Collaboration (S. Afanasiev *et al.*), «Systematic studies of elliptic flow measurements in Au+Au collisions at $\sqrt{s_{NN}} = 200$ GeV», *Phys. Rev. C* **80**, 024909 (2009).

[32] PHENIX Collaboration (A. Adare *et al.*), «Systematic study of charged-pion and kaon femtoscopy in Au+Au collisions at $\sqrt{s_{NN}} = 200$ GeV», *Phys. Rev. C* **92**, 034914 (2015).

[33] S. Pratt *et al.*, «Testing transport theories with correlation measurements», *Nucl. Phys. A* **566**, 103c (1994).

[34] PHENIX Collaboration (S.S. Adler *et al.*), «Bose–Einstein Correlations of Charged Pion Pairs in Collisions at», *Phys. Rev. Lett.* **93**, 152302 (2004).